J Mol Model (2012) 18:3415–3425
DOI 10.1007/s00894-012-1352-0

ORIGINAL PAPER

Can *trans*-polyacetylene be formed on single-walled carbon-doped boron nitride nanotubes?

Ying Chen · Hong-xia Wang · Jing-xiang Zhao · Qing-hai Cai · Xiao-guang Wang · Xuan-zhang Wang

Received: 7 November 2011 / Accepted: 1 January 2012 / Published online: 21 January 2012

Abstract Recently, the grafting of polymer chains onto nanotubes has attracted increasing attention as it can potentially be used to enhance the solubility of nanotubes and in the development of novel nanotube-based devices. In this article, based on density functional theory (DFT) calculations, we report the formation of *trans*-polyacetylene on single-walled carbon-doped boron nitride nanotubes (BNNTs) through their adsorption of a series of C_2H_2 molecules. The results show that, rather than through [2+2] cycloaddition, an individualmolecule would preferentially attach to a carbon-doped BNNT via "carbon attack" (i.e., a carbon in the C_2H_2 attacks a site on the BNNT). The adsorption energy gradually decreases with increasing tube diameter. The free radical of the carbon-doped BNNT is almost completely transferred to the carbon atom at the end of the adsorbed C_2H_2 molecule. When another C_2H_2 molecule approaches the carbon-doped BNNT, it is most energetically favorable for this C_2H_2 molecule to be adsorbed at the end of the previously adsorbed C_2H_2 molecule, and so on with extra C_2H_2 molecules, leading to the formation of polyacetylene on the nanotube. The spin of the whole system is always localized at the tip of the polyacetylene formed, which initiates the adsorption of the incoming species. The present results imply that carbon-doped BNNT is an effective "metal-free" initiator for the formation of polyacetylene.

Keywords Polyacetylene · Carbon-doped boron nitride nanotubes · DFT

Introduction

Since the pioneering report on the synthesis of carbon nanotube (CNT)–polymer composites by Ajayan et al. in 1994 [1], considerable efforts have been made to fabricate and develop nanotube-based polycomposites [2]. This is understandable because the long polymer chains help the nanotubes to dissolve in various solvents, even with only a low degree of functionalization [3], and, compared to unprocessed polymers and nanotubes, these nanocomposites have more useful or enhanced electrical and optical properties, thermal conductivities, and superior mechanical strengths [4–9]. These remarkable properties have stimulated great interest, and make them potential candidates for use in high-efficiency photovoltaic cells and light-emitting devices, as reinforcing fibers in superstrong composites, and so on [10–13].

Like carbon nanotubes, boron nitride (BN) can also form one-dimensional nanostructures—boron nitride nanotubes (BNNTs) [14]. Although BN is isoelectronic with a pair of carbon atoms, the electronic properties of these pairs of atoms are completely different: CNTs show metallic or semiconducting properties, while BNNTs are large band-gap (almost always ~5.8 eV) semiconductors that preferably form zigzag structures which are more stable than CNTs in terms of thermal and chemical stability [15–17]. In particular, due to

Electronic supplementary material The online version of this article (doi:10.1007/s00894-012-1352-0) contains supplementary material, which is available to authorized users.

Y. Chen · H.-x. Wang · J.-x. Zhao (✉) · Q.-h. Cai · X.-g. Wang · X.-z. Wang
Key Lab for Design & Synthesis of Functionalized Materials and Green Catalysis, School of Chemistry and Chemical Engineering, Harbin Normal University,
Harbin 150025, People's Republic of China
e-mail: xjz_hmily@yahoo.com.cn

their superb mechanical properties and high thermal conductivities, boron nitride nanotubes are potentially applicable in the design of nanotube–polymer composites that can be used in oxidative and hazardous environments or at high temperatures [18, 19]. Unlike CNT–polymer composites, however, to the best of our knowledge, not much attention has been given to the covalent interactions of polymer composites with BNNTs [20, 21], especially the process of grafting polymers to BNNTs. In an attempt to elucidate BNNT–polymer formation, we chose to study the attachment of the relatively simple molecule C_2H_2 to a BNNT, which enabled us to explore the bonding, geometry, and stability of polyacetylene (with its unique electronic, optical, and electroluminescent properties [22–24]) on BNNTs. In particular, the work addressed the following questions. (1) How does C_2H_2 polymerization on carbon-doped BNNT proceed? (2) Why can carbon-doped BNNT initiate C_2H_2 polymerization? (3) What is the effect of the tube diameter on C_2H_2 polymerization? (4) How do the electronic properties of a carbon-doped BNNT change after polyacetylene has been grafted onto it?

Computational methods and models

Density functional theory (DFT) calculations were performed using the double numerical plus polarization (DNP) basis set, which is implemented in the DMol^3 package [25, 26]. The generalized gradient approximation (GGA) of Perdew–Burke–Ernzerhof (PBE) was employed to obtain all of the results given below [27]. Since BNNTs preferentially adopt zigzag chirality during growth [28–30], we only investigated zigzag (n, 0) (n=8, 9, 10, 11, and 15) nanotubes. A cluster model was built to study the formation of polyacetylene on carbon-doped BNNTs. Each BNNT included three unit cells for the zigzag tube [for example, 48 B and 48 N atoms for an (8, 0) BNNT]. Hydrogen atoms were used to avoid the effects of dangling bonds at the two ends. For comparison, we also studied C_2H_2 polymerization on a hexagonal BN graphene sheet using a 5×5 supercell in two dimensions, which had edges saturated with hydrogen atoms, as shown in Fig. S1 of the "Electronic supplementary material," ESM.

The adsorption (or interaction) energy per C_2H_2 molecule adsorbed onto the carbon-doped BNNT was defined as

$$E_{ads} = [E_{total}(\text{tube}/N - C_2H_2) - E_{total}(\text{tube}) - NE_{total}(C_2H_2)]/N, \quad (1)$$

where $E_{ads}(N)$ is the average adsorption energy of N C_2H_2 molecules on carbon-doped BNNTs, E_{total} is the total energy of the systems in parentheses, and n is the number of adsorbed C_2H_2 molecules. A negative value of E_{ads} corresponds to a stable adsorption structure. If we suppose that these C_2H_2 molecules are adsorbed one by one, the adsorption energy of the Nth C_2H_2 molecule on doped BNNT can be written as

$$E_{ads}(N\text{th}) = E_{ads}(N) - E_{ads}(N-1) \quad (2)$$

$$= [E_{total}(\text{tube}/N - C_2H_2) - E_{total}(\text{tube}) - NE_{total}(C_2H_2)] - [E_{total}(\text{tube}/(N-1) - C_2H_2) - E_{total}(\text{tube}) - (N-1)E_{total}(C_2H_2)] \quad (3)$$

$$= [E_{total}(\text{tube}/N - C_2H_2)] - [E_{total}(\text{tube}/(N-1) - C_2H_2)] - E_{total}(C_2H_2). \quad (4)$$

Results and discussion

Adsorption of an individual C_2H_2 molecule

First, we investigated the adsorption of an individual C_2H_2 molecule onto carbon-doped BNNT. In the carbon-doped BNNT, a boron (in a "C_B-doped" BNNT) or nitrogen (in a "C_N-doped" BNNT) atom is substituted by a carbon atom. For simplicity, a C_B-doped (8, 0) BNNT is used here as an example. For this doped BNNT, structural relaxation results in a small outward displacement along the radial direction, which facilitates C_2H_2 adsorption due to decreased steric hindrance from the BNNT sidewall. The average C–N distance is shortened by ~0.027 Å compared to the B–N distance in pristine BNNT (1.448 Å). Figure 1 plots spin density, the highest occupied molecular orbital (HOMO), the lowest unoccupied molecular orbital (LUMO), and the Fukui functions [31]. We found that the calculated spin density, HOMO, LUMO, and Fukui functions are strongly localized at the introduced C impurity. Hence, the site of the C impurity exhibits much higher reactivity towards adsorbates than the other atoms in the doped BNNT.

For the adsorption of an individual C_2H_2 onto the C_B (8, 0) BNNT, two kinds of initial adsorption configuration are conceivable: the C_2H_2 molecule attaches to the doped BNNT through "carbon attack" or [2+2] cycloaddition. In the former, one of the carbon atoms of the linear C_2H_2 molecule vertically attacks the C impurity, the boron, or the nitrogen site of the doped BNNT. In the latter, the C–C bond of the C_2H_2 molecule is adsorbed onto the C–N or B–N bond of the doped BNNT via [2+2] cycloaddition, resulting in the formation of a four-membered ring. The C-doped BNNT has a ground state of S=1/2, so we performed spin-polarized calculations for those configurations.

After carefully optimizing the structure of each initial adsorptive configuration by varying its spin multiplicity, it

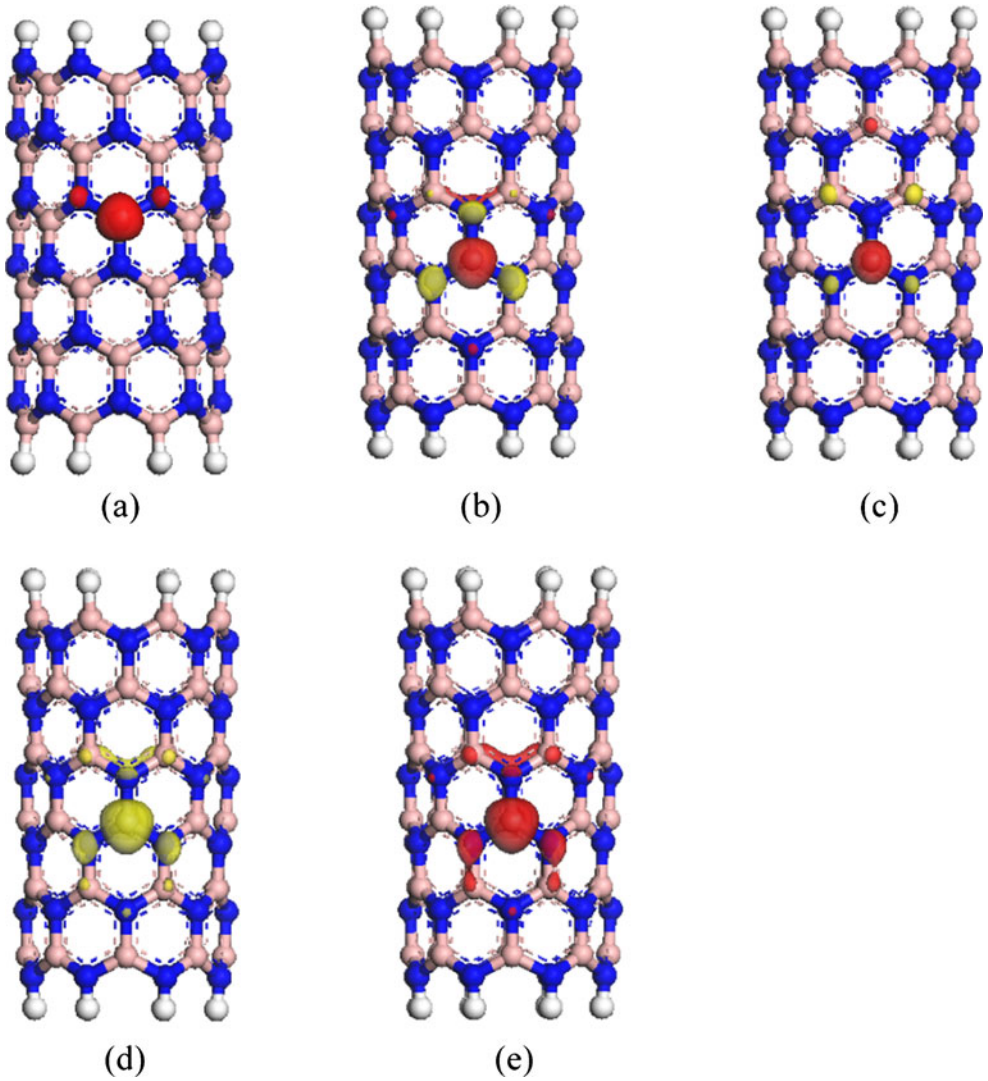

Fig. 1 **a** Spin density, **b** HOMO, **c** LUMO, **d** Fukui functional $f^-(r)$, and **e** Fukui functional $f^+(r)$ of a C_B-doped (8, 0) BNNT

was found that it is most energetically favorable for the C_2H_2 molecule to attach to the doped BNNT through carbon attack. Here, the doublet state is the ground state. For the most stable configuration (Fig. 2a), one carbon atom of C_2H_2 is bound to the C impurity of the C_B (8, 0) BNNT, while the other carbon atom is far from the nanotube. This configuration has an E_{ads} value of −0.661 eV, and the distance between the C_2H_2 and the doped BNNT is 1.549 Å. The two H atoms of the adsorbed C_2H_2 molecule are on either side of the C–C bond. PBE/TNP calculations were also performed for this configuration (Fig. 2a), and the resulting geometric structure is shown in Fig. S2 of the ESM. We found that the results from the PBE/DNP and PBE/TNP calculations were quite similar, except that the E_{ads} value calculated using PBE/TNP is slightly larger (−0.710 eV). Thus, the method used in the present work is accurate enough to study the adsorption of C_2H_2 onto a C-doped BNNT. Furthermore, this adsorption induces local structural deformation of both the C_2H_2 molecule and the C_B (8, 0) BNNT (Fig. 2a): (i) the length of the C–C bond of C_2H_2 increases from 1.211 (free C_2H_2) to 1.311 Å, while the bond angles H–C–C of C_2H_2 decrease significantly from 180° to 121° and 140° in the adsorbed form. The adsorbed C-impurity site on the C_2H_2 molecule is pulled outward from the tube surface, and the C–N bond lengths are 1.473, 1.493, and 1.493 Å, respectively, which are larger than those in the original C_B (8, 0) BNNT (1.407, 1.428, and 1.428 Å, respectively). Such structural deformation can be attributed to the change in the local hybridization of the carbon impurity in the doped BNNT from an sp^2 to an sp^3 orbital, implying that the adsorption is covalent. More interestingly, the magnetic moment (0.784 μ_B using the Hirshfeld method, Fig. S3 in Supporting Information) of this nanocomposite is localized on the carbon atom at the end of the adsorbed C_2H_2 molecule. In other words, the spin of the C_B-doped BNNT is almost completely transferred tothe adsorbed C_2H_2 molecule. Hence, the carbon atom at the tip of the adsorbed C_2H_2 molecule possesses high reactivity

toward incoming adsorbates, and provides a greater contribution to the HOMO, LUMO, and Fukui functions (Fig. S3) than the other atoms of the system. In addition, four other metastable adsorption configurations are obtained, as shown in Fig. 3b–e. The calculated adsorption energies are −0.658 (Fig. 2b), −0.651 (Fig. 2c), −0.649 (Fig. 2d), and −0.195 eV (Fig. 2e), respectively.

For these metastable configurations, it was consistently found that (i) the carbon-attack configurations of the C_2H_2 molecule on the C_B-doped BNNT (Fig. 2b–d) are more stable than those of [2+2] cycloaddition (Fig. 2e), (ii) the adsorption of an individual C_2H_2 molecule on a C_B (8, 0) BNNT is nearly independent of its orientation with respect to the nanotube (Fig. 2a and b), and (iii) it is slightly more stable for the two

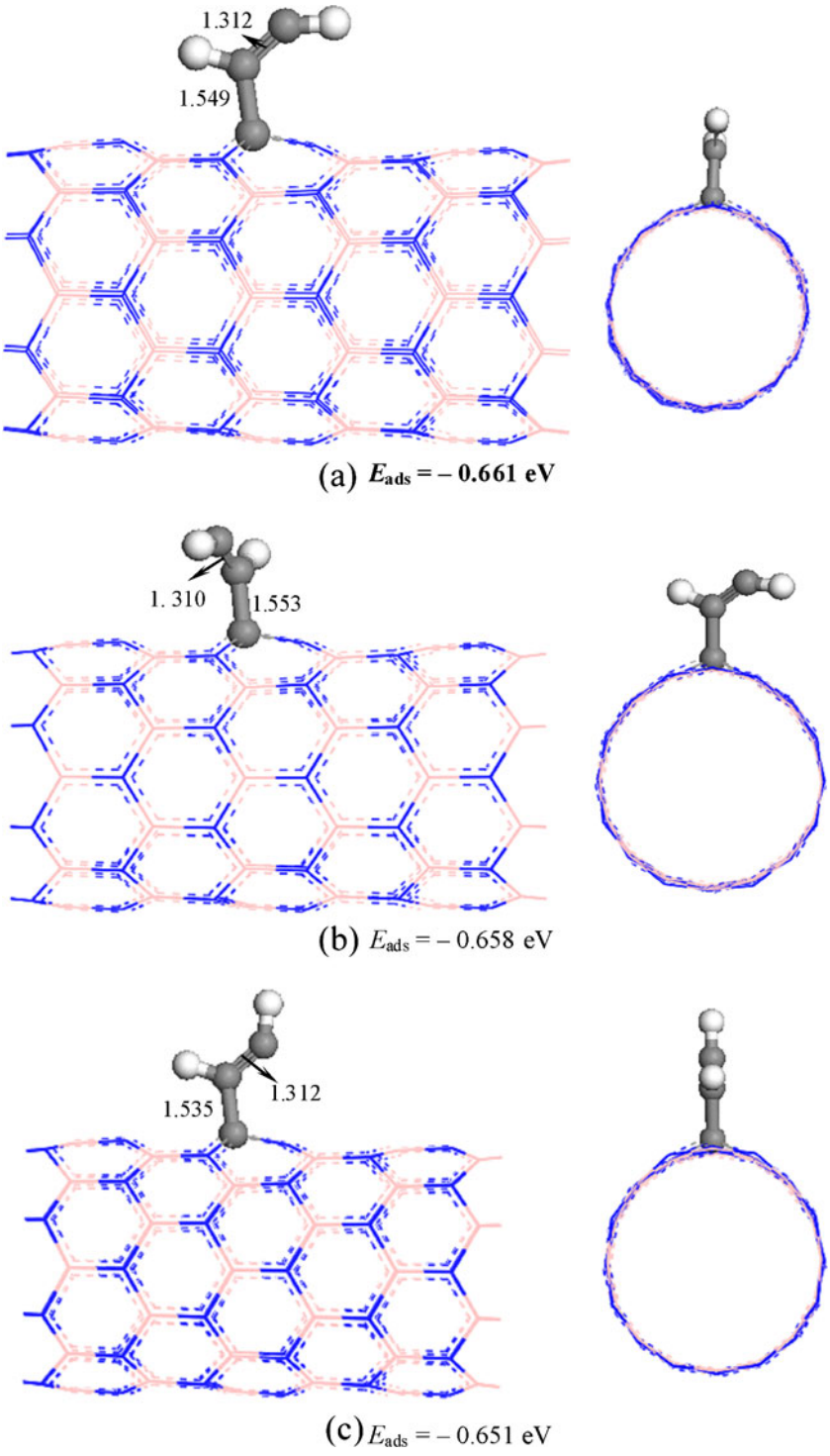

Fig. 2 **a–e** Optimized structure of an individual C_2H_2 molecule on a C_B-doped (8, 0) BNNT. Various adsorption sites and C_2H_2 orientations were examined. The bond distances are in angstroms

Fig. 2 (continued)

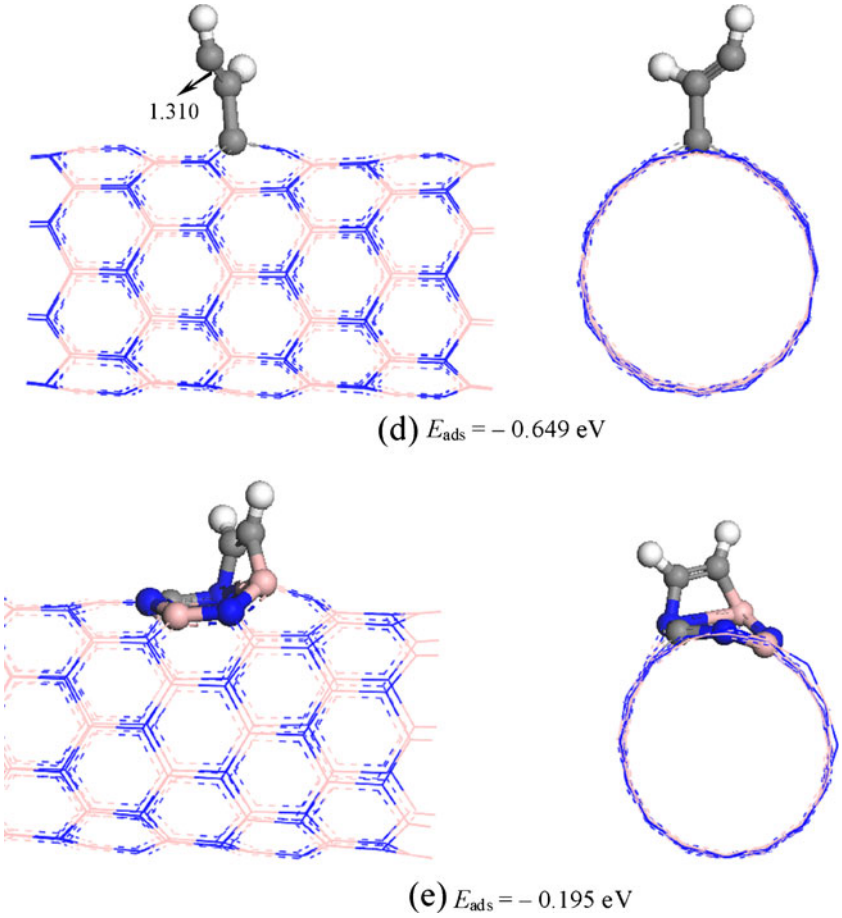

hydrogen atoms of the adsorbed C_2H_2 molecule to be located on both sides (Fig. 2a and b) of the C–C bond than on the same side (Fig. 2c and d).

To evaluate the effect of the curvature of the C_B-doped BNNT on individual C_2H_2 adsorption, we calculated the attachment of a single C_2H_2 molecule to other zigzag C_B (n, 0) (n=9, 10, 11, and 15) BNNTs and C_B BN graphene. For simplicity, only the carbon-attack configuration shown in Fig. 2a was considered. In Fig. 3, we present curves of the calculated adsorption energy with n for carbon-doped BNNTs. Clearly, C_2H_2 adsorption gradually weakens with increasing tube diameter due to curvature effects. For example, the adsorption energy of C_2H_2 on a (9, 0) tube is −0.654 eV, while it decreases to −0.421 eV on C_B-doped BN graphene. This indicates that the C_2H_2 molecule can be stably chemisorbed on all of the C_B-doped BNNTs investigated, as well as on BN graphene, and that in all cases the adsorption is accompanied by near-complete spin transfer from the nanotube to the adsorbed C_2H_2 molecule.

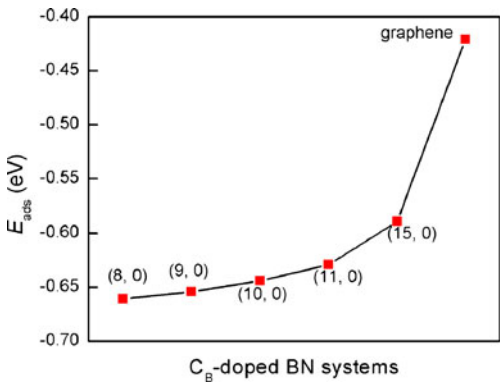

Fig. 3 The adsorption energies of an individual C_2H_2 molecule on C_B-doped (n, 0) BNNTs (n=8, 9, 10, 11, 15) and BN graphene

The formation of *trans*-polyacetylene on carbon-doped BNNTs

Based on the above results for individual C_2H_2 molecule adsorption, we further investigated the formation of *trans*-polyacetylene on carbon-doped BNNTs.

When two C_2H_2 molecules are adsorbed onto a C_B-doped (8, 0) BNNT, a number of configurations are possible. The two C_2H_2 molecules could be co-adsorbed through carbon attack, [2+2] cycloaddition, carbon attack by one molecule and [2+2] cycloaddition by the other molecule, or polymerization (the second C_2H_2 is adsorbed onto the first C_2H_2). Among the locally stable configurations shown in Fig. 4, the

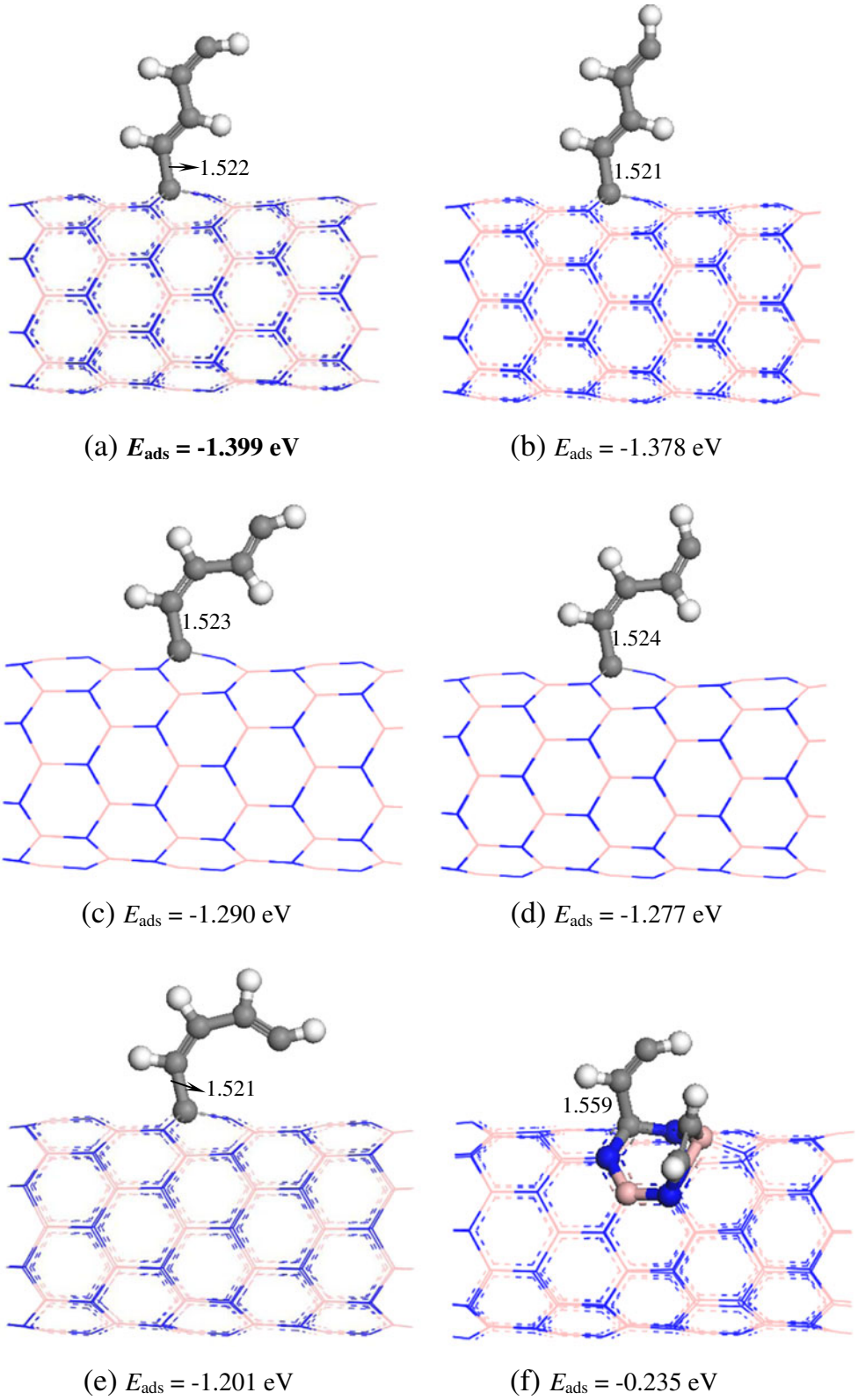

(a) E_{ads} = **-1.399 eV** (b) E_{ads} = -1.378 eV

(c) E_{ads} = -1.290 eV (d) E_{ads} = -1.277 eV

(e) E_{ads} = -1.201 eV (f) E_{ads} = -0.235 eV

Fig. 4 **a–i** Optimized structures of two C_2H_2 molecules on a C_B-doped (8, 0) BNNT. Various adsorption sites and C_2H_2 orientations were examined. The bond distances are in angstroms

most energetically preferred is the one where the carbon atom of the second C_2H_2 binds with the carbon atom at the end of the first C_2H_2 molecule (Fig. 4a); i.e., the two monomer molecules dimerize to produce a dimer, the *trans*-C_4H_4 species. This further suggests that the carbon atom at the end of the first C_2H_2 molecule has a much higher

Fig. 4 (continued)

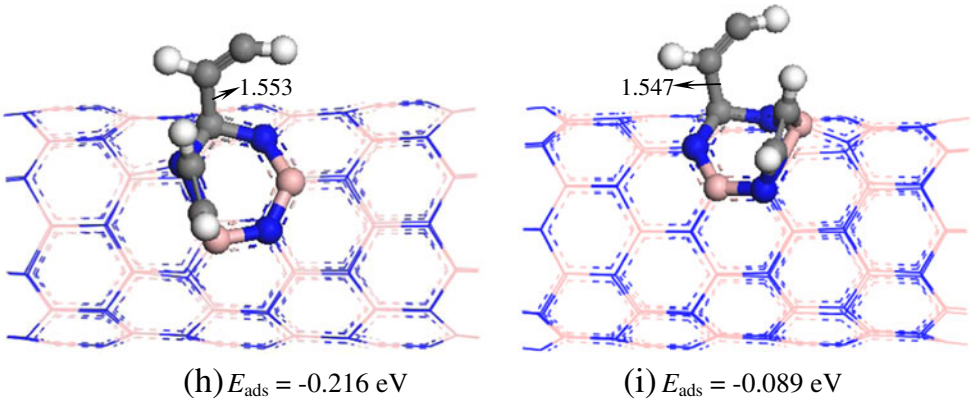

Fig. 5 Optimized structures of **a** three, **b** four, **c** five, **d** six, **e** seven, and (**f**) eight C_2H_2 molecules on a C_B-doped (8, 0) BNNT. The bond distances are in angstroms

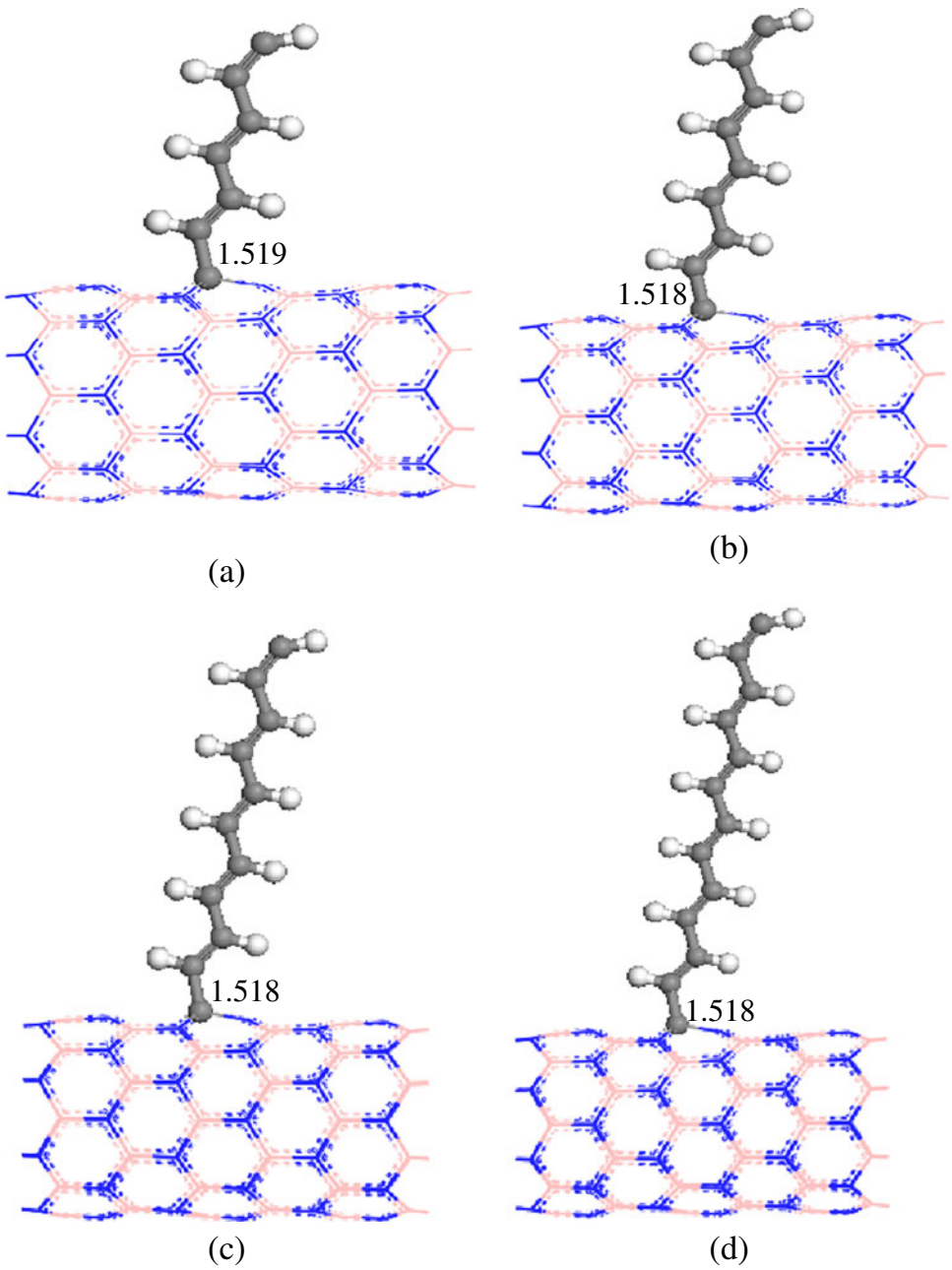

Fig. 5 (continued)

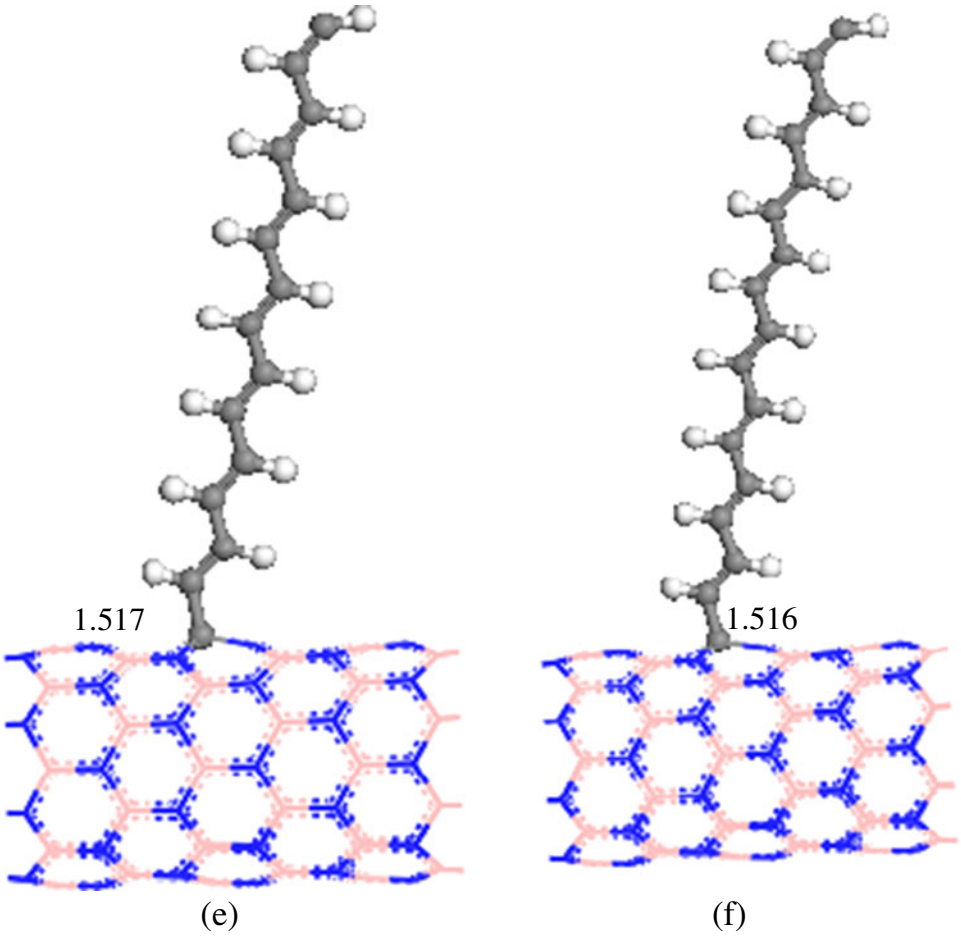

reactivity than the other atoms. The adsorption energy of this configuration is −1.399 eV per C_2H_2 molecule according to Eq. 1, which is roughly twice an individual energy of C_2H_2 adsorption (−0.661 eV). The distance between the two adsorbed C_2H_2 molecules is 1.463 Å, while the C–C bonds of the two C_2H_2 molecules increase to 1.346 and 1.326 Å, respectively. Similar to the case for individual C_2H_2 adsorption, the spin density, HOMO, LUMO, and Fukui functions of this most stable configuration receive the greatest contributions from the carbon atom at the tip of the *trans*-C_4H_4 species (see Fig. S4 of the ESM), indicating that it is the most reactive region for subsequent adsorbates. In addition to the lowest-energy configuration, we also obtained other seven metastable adsorption configurations with adsorption energies ranging from −0.089 eV (Fig. 4i) to −1.378 eV (Fig. 4b). We should point out that the configurations for C_2H_2 dimerization on the carbon-doped (8, 0) BNNT (Fig. 4a–e) are much more energetically favorable than the others (Fig. 4f–i).

To gain deeper insight into the behavior of multiple C_2H_2 molecules on the carbon-doped BNNT, we gradually increased the number of C_2H_2 molecules from 3 to 8 on the nanotube. The structures obtained are shown in Fig. 5. We found that the *N*th C_2H_2 molecule always prefers to bind with the tip of the $(N-1)$th C_2H_2 molecule, where *N* is the number of C_2H_2 molecules adsorbed onto the doped BNNT, leading to the formation of a *trans*-polyacetylene system on the nanotube, as shown in Scheme 1. We also found that the spin of the whole system is always localized at the tip of the formed *trans*-polyacetylene species. Due to the high reactivity of the chain tip, NC_2H_2/nanotube systems can initiate some important reactions, such as the oxidation of hydrocarbons.

In Fig. 6, we present the variation of the calculated adsorption energy (E_{ads}) with the number of C_2H_2 molecules adsorbed (*N*) onto various carbon-doped BN systems. The results indicate that the E_{ads} values of the C_2H_2 molecules on these BN systems decrease linearly with increasing *N*. Also, the E_{ads} values of the C_2H_2 molecules on the C_B-doped (8, 0) BNNT are slightly larger than those on the C_B-doped BN graphene, suggesting that C_2H_2 polymerization on carbon-doped BN systems is almost independent of tube size. In other words, it is very easy for C_2H_2 molecules to polymerize on C_B-

Scheme 1 The polymerization of C_2H_2 molecules on carbon-doped BNNT

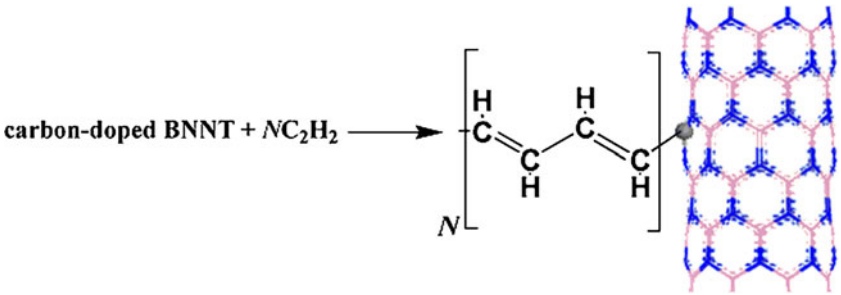

doped BN nanostructures. C_2H_2 molecules can also polymerize on C_N-doped BNNTs, and their interactions with this type of doped BNNT are somewhat stronger than those of C_B-doped BNNTs. Finally, the general trend in the E_{ads} values for C_2H_2 obtained using Eq. 1 is consistent with that seen when using Eq. 4, although the values obtained with the latter are obviously larger than those gained with the former.

Although our study is based on a cluster model, we expect that similar conclusions will be obtained for periodic systems. Toward this end, we have performed several test calculations on the periodic zigzag (8, 0) BNNT, in which a one-dimensional (1D) periodic boundary condition was applied along the tube axis to simulate an infinitely long (rather than truncated) nanotube. A hexagonal supercell of size 30×30× 12.78 $Å^3$ was adopted, which is enough large to avoid interactions of C_2H_2 with its periodic images. Moreover, the length of the tube axis is three times the periodic length of the zigzag (8, 0) BNNT. The PBE/DNP method was adopted for the calculations. After geometric optimization, we found that the structures obtained exhibited the same configurations as those in the cluster model. The adsorption energies are summarized in Table 1, where a similar trend to that obtained in the cluster model is apparent.

Finally, we use C_B-doped (8, 0) BNNT as an example to explore the effects of grafting N C_2H_2 molecules (N=1–8) onto the nanotube on its electronic properties. Accordingly, the calculated band structures for the pristine and functionalized BNNTs are shown in Fig. 7, and the obtained band gaps are presented in Table 1. For the C_B-doped (8, 0) BNNT, the C impurity introduces two levels into the band gap (Fig. 7a): the spin-up level is deep inside the band gap, while the spin-down level is 0.841 eV above the bottom of the conduction band, which is in agreement with previous studies [32, 33]. The local density of states (LDOS) in Fig. 7b indicates that the sharp peak near the Fermi level in the total density of states (TDOS) is contributed by the C impurity. Upon grafting N C_2H_2 molecules (N=1~8) onto the C_B-doped (8, 0) BNNT, as shown in Fig. 7c–e, we found that more band levels are introduced into the band structure, and the band gap of doped BNNT is increased by different amounts because the spin-down level above the bottom of the conduction band is lifted up by different degrees with

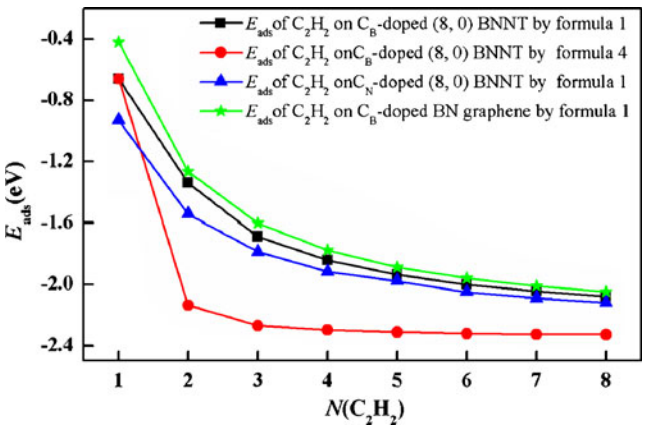

Fig. 6 Variation in adsorption energy (per C_2H_2 molecule) as a function of the number of C_2H_2 molecules adsorbed onto a C_B-doped (8, 0) BNNT

Table 1 Average adsorption energies[a] of N C_2H_2 (N=1–8) molecules adsorbed onto a zigzag C_B-doped (8, 0) BNNT, and the band gaps of the resulting composites, calculated using a periodic model

N C_2H_2 molecules	E_{ads} (eV)[2]	Band gap (eV)
1	−0.648 (−0.661)	2.171
2	−1.389 (−1.399)	2.479
3	−1.680 (−1.690)	2.196
4	−1.833 (−1.842)	1.948
5	−1.928 (−1.936)	1.772
6	−1.991 (−2.000)	1.646
7	−2.037 (−2.047)	1.550
8	−2.069 (−2.081)	1.405
C_B-doped (8, 0) BNNT	-	0.841

[a] The average adsorption energies were calculated according to Eq. 1

[b] The E_{ads} value in parentheses was calculated using the cluster model

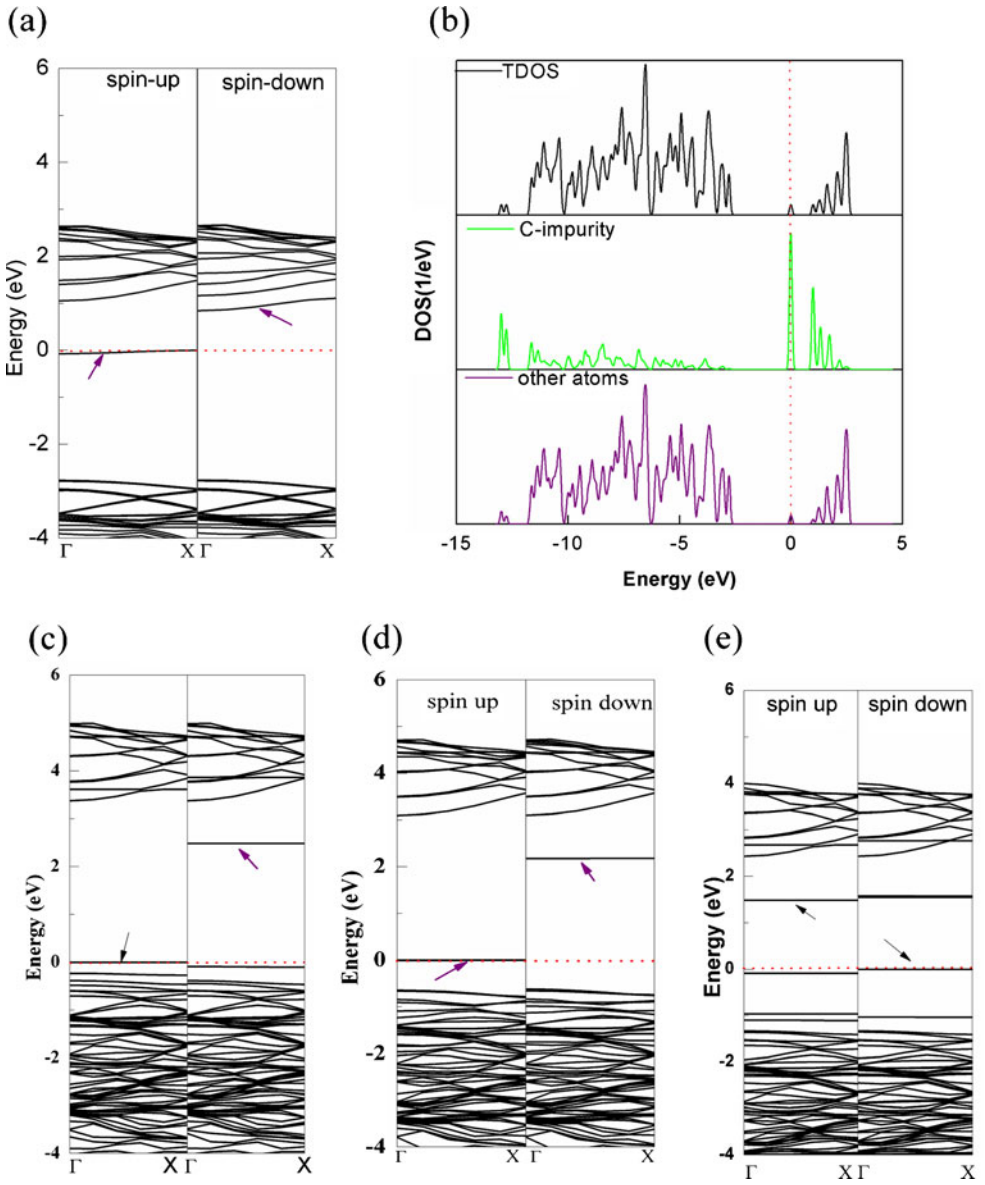

Fig. 7 The band structures of N C_2H_2/C_B-doped (8, 0) BNNT for **a** N=0, **c** N=1, **d** N=2, **e** N=7. **b** The total and local densities of states for the C_B-doped (8, 0) BNNT. The Fermi level is shown by a *red dotted line*

different values of N. For example, when one, two, or seven C_2H_2 molecules are attached to the C_B-doped (8, 0) BNNT, the band gap increases by 1.330, 1.638, and 0.709 eV, respectively, as shown in Table 1. In particular, the spin-down level of the C_B-doped (8, 0) BNNT is lifted to the greatest extent when two C_2H_2 molecules are adsorbed, thereby leading to the largest band gap for N = 2 (Table 1).

Clearly, our DFT calculations show that the C_B-doped BNNT is an ideal "metal-free" initiator for the formation of polyacetylene. Remarkably, this initiator (substituted carbon-doped BN nanostructures) has been recently achieved via in situ electron beam irradiation in an energy-filtering 300 kV high-resolution transmission electron microscope [34]. In this sense, our study provides valuable guidance for finding an effective initiator for C_2H_2 polymerization.

Conclusions

In conclusion, ab initio calculation results suggest that *trans*-polyacetylene is easily formed on carbon-doped BNNT. The mechanism of C_2H_2 polymerization is attributed to continuous spin transfer from the BNNT to the most recently adsorbed C_2H_2 molecule. After grafting C_2H_2 molecules onto the doped BNNT, the band gap of the nanotube is increased to various extents depending on how the band structure is calculated. Finally, we are actively investigating the potential of the carbon-doped BNNT as an initiator for

the polymerization of other polyenes with π-conjugated backbones (such as ethylene and butadiene).

Acknowledgments This work is supported by the China Postdoctoral Science Foundation (no. 20110491119), Committee of Education of Heilongjiang Province (no. 11541095), the Natural Science Foundation of Heilongjiang Province (no. B201011), the Key Project of Chinese Ministry of Education (no. 210060), and the Scientific Research Foundation for Doctor of Harbin Normal University (no. 08XKYL38). The authors express their greatest gratitude to the reviewers for their invaluable comments and suggestions.

References

1. Ajayan PM, Stephan O, Colliex C, Trauth D (1994) Science 265:1212–1214
2. Sahoo NG, Rana S, Cho JW, Li L, Chan SH (2010) Prog Polym Sci 35:837–867, and references therein
3. Tasis D, Tagmatarchis N, Bianco A, Prato M (2006) Chem Rev 106:1105–1136
4. Spitalsky Z, Tasis D, Papagelis K, Galiotis C (2010) Prog Polym Sci 35:357–401
5. Du J-H, Bai J, Cheng HM (2007) Express Polym Lett 1:253–273
6. Moniruzzaman M, Winey KI (2006) Macromolecules 39:5194–5205
7. Lu XF, Zhang WJ, Wang C, Wen TC, Wei Y (2011) Prog Polym Sci 36:671–712
8. Coleman JN, Khan U, Blau BJ, Gun'ko YK (2006) Carbon 44:1624–1652
9. Rozenberg BA, Tenne R (2008) Prog Polym Sci 33:40–112
10. Ma PC, Siddiqui NA, Marom G, Kim JK (2010) Composites 41:1345–1367
11. Wernik JM, Meguid SA (2010) Appl Mech Rev 63:050801-1-40
12. In het Panhuis M (2006) J Mater Chem 16:3598–3605
13. Hasan T, Sun Z, Wang F, Bonaccorso F, Tan PH, Rozhin AG, Ferrari AC (2009) Adv Mater 21:3874–3899
14. Rubio A, Corkill JL, Cohen ML (1994) Phys Rev B 49:5081–5084
15. Chopra NG, Luyken RJ, Cherrey K, Crespi VH, Cohen ML, Louie SG, Zettl A (1995) Science 269:966–967
16. Loiseau A, Willam F, Demoncy N, Hug G, Pascard H (1996) Phys Rev Lett 76:4737–4740
17. Xiang JH, Yang LJ, Hou JG, Zhu SQ (2003) Phys Rev B 68:035427
18. Golberg D, Bando Y, Tang CC, Zhi CY (2007) Adv Mater 19:2413–2432
19. Zhi CY, Bando Y, Tang CC, Goberg D (2010) Mater Sci Eng R 70:92–111
20. Zhi CY, Bando Y, Tang CC, Xie RG, Sekiguchi T, Golberg D (2005) J Am Chem Soc 127:15996–15997
21. Zhi YC, Bando Y, Tang CC, Kuwahara H, Golberg D (2007) J Phys Chem C 111:1230–1233
22. Skotheim TA (ed) (1986) Handbook of conducting polymers. Marcel Dekker, New York
23. Nalwa HS (ed) (1997) Handbook of organic conductive molecules and polymers. Wiley, New York
24. Akagi K, Shirakawa H (1998) In: Wise DL, Wnek GE, Trantolo DJ, Cooper TM, Gresser JD (eds) Electrical and optical polymer systems: fundamentals, methods, and applications. Marcel Dekker, New York, p 983
25. Delley B (1990) J Chem Phys 92:508–517
26. Delley B (2000) J Chem Phys 113:7756–7764
27. Perdew JP, Burke K, Ernzerhof M (1996) Phys Rev Lett 77:3865–3868
28. Golberg D, Bando Y (2001) Appl Phys Lett 79:415–417
29. Ma RZ, Bando Y, Sato T, Kurashima K (2001) Chem Mater 13:2965–2971
30. Lee RS, Gavillet J, de la Chapelle ML, Loiseau A, Cochon JL, Pigache D, Thibault J, Willaime F (2001) Phys Rev B 64:121405
31. Parr RG, Yang W (1989) Density-functional theory of atoms and molecules. Oxford University Press, New York
32. Schmidt TM, Bailerle RJ, Piquini P, Fazzio A (2003) Phys Rev B 67:113407
33. Baierle RJ, Piquini P, Schmidt TM, Fazzio A (2006) J Phys Chem B 110:21184–21188
34. Wei X, Wang M-S, Bando Y, Golberg D (2011) ACS Nano 5:2916–2922